IL NUOVO CIMENTO Vol. 35 C, N. 5 Settembre-Ottobre 2012
DOI 10.1393/ncc/i2012-11305-7

Communications: SIF Congress 2011

Central collisions in $^{58}\mathrm{Ni} + {}^{48}\mathrm{Ca}$ system with CHIMERA at 25 AMeV

L. Francalanza(*)

INFN, Laboratori Nazionali del Sud - Catania, Italy

ricevuto il 31 Dicembre 2011; revisionato il 14 Aprile 2012; approvato il 23 Aprile 2012
pubblicato online il 6 Settembre 2012

Summary. — The central collisions of $^{58}\mathrm{Ni} + {}^{48}\mathrm{Ca}$ reactions at $E_{\mathrm{lab}}(\mathrm{Ni}) = 25\,A\mathrm{MeV}$, have been studied using the CHIMERA 4π array, in order to investigate the competition between different reaction mechanisms. To select central collisions, the kinetic energy tensor and the "flow angle" in an event-by-event analysis are used. The main features of the reaction products have been studied and some global observable and their correlations, capable to characterize the pattern of central collisions, are shown. In particular, strong evidence for the competition between fusion-evaporation processes, with consequent identification of heavy residue and multifragmentation reaction mechanism are reported.

PACS 25.70.-z – Low and intermediate energy heavy-ion reactions.
PACS 25.70.Pq – Multifragment emission and correlations.

1. – Introduction

Nuclear reactions induced by heavy ions around the Fermi energy domain (40 MeV/nucleon) are characterized by a transition from the mean field dissipation mechanism (one-body), dominating at bombarding energies close to the Coulomb barrier between the two interacting nuclei, to the nucleon-nucleon interaction process (two body), that is the dominant mechanism in reactions at beam energies above the Fermi domain.

One clear experimental signature of this transition mechanism was found in the early 1980s, with the observation of a copious production of Intermediate Mass Fragments (IMF, fragments with charge $Z > 2$) in central collisions. The multiplicity of IMFs was observed to be more than one order of magnitude larger than that expected in the de-excitation of an equilibrated nuclear system produced in fusion-evaporation reactions. To explain the observed new multifragmentation process, different scenarios have been proposed. The existing models range from prompt dynamical emissions, simulated in

(*) E-mail: francalanza@lns.infn.it

the contest of transport theories, to statistical multifragmentation emissions in a low density and short-lived nuclear system at chemical equilibrium [1]. More recently, with the advance of a new generation of 4π detectors [2], multifragmentation phenomena have been observed in complex reactions where a coexistence of both dynamical and statistical emissions of fragments takes place on comparably short time-scales. Therefore, these studies offer unique opportunities to better understand the evolution of the many-body nuclear systems under different experimental conditions. Studying multifragmentation processes as a function of impact parameter, relative kinetic energy and size of interacting ions, is important in order to disentangle among different reaction mechanisms, ranging from the quasi-elastic to the most dissipative collisions. In particular, intermediate energy collisions at small impact parameters is of great interest because it allows us to study reactions where maximum transferred linear momentum and formation of single highly excited sources is expected to occur.

In this article, a careful selection of central collisions in the reaction ^{58}Ni + ^{48}Ca [3] is described in order to investigate the competition between sequential fusion-evaporation and prompt multifragmentation decay of an unstable system formed at sub-saturation nuclear density.

2. – The experiment

The experiment was performed at the INFN-Laboratori Nazionali del Sud, with ion beams of ^{58}Ni accelerated at 25 AMeV by the LNS Superconducting Cyclotron, impinging on a thin ^{48}Ca target, sandwiched between two very thin carbon foils in order to reduce oxidation. Reaction products were then detected using the 1192 silicon-CsI(Tl) telescopes of the CHIMERA 4π multidetector, covering almost 94% of the total solid angle [4, 5]. CHIMERA's ΔE-E identification technique allows determination of the atomic number Z of the reaction products punching through the silicon detectors and stop in the CsI(Tl) crystals as well as the charge and mass of those fragments with $3 \leq Z \leq 8$, detected at laboratory angles larger than 13°. Particle velocities were measured by a time-of-flight (TOF) technique, performed using the cyclotron radio frequency, as a start reference time, and the silicon time signal as stop. Combining the information from these two identification methods, it was possible to evaluate the mass of particles stopped in silicon detectors. For the present analysis, the identification of light charged particles by means of a Pulse Shape Discrimination (PSD) technique has not been included, which only slightly affects the global reconstruction of the reaction pattern, made on an event-by-event basis. Events were registered when the silicon detectors of at least two telescopes were fired (charged particle multiplicity, $M_{\mathrm{CP}} \geq 2$). Two relevant quantities in the present work are the projectile velocity, $v_{\mathrm{proj}} \approx 6.5\,\mathrm{cm/ns}$, and the centre of mass velocity, $v_{\mathrm{CM}} \approx 3.8\,\mathrm{cm/ns}$, evaluated for the binary system indicated above.

3. – Data analysis: Event selection and characterization

3˙1. *Complete events.* – Only those "complete events", where the total collected charge ranged between the 70% and 105% of the total charge in the entrance channel, were selected for off-line analysis. A similar condition was also imposed on the total measured longitudinal momentum (*i.e.* the projection of the total momentum on the beam axis) with respect to the linear momentum of the projectile. In this way 11.5% of total events were selected as complete events (see region in square box in fig. 1).

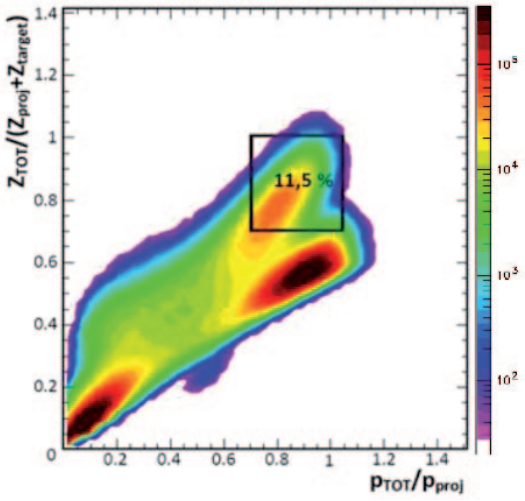

Fig. 1. – Correlation between total detected charge and total longitudinal momentum for all detected events. Events in the square box (11.5% of total events) were selected as complete events.

In order to characterize complete events it is useful to describe them with some global variables, like charged particle multiplicity, $M_{\rm CP}$, fragments multiplicity, $M_{\rm IMF}$, total kinetic energy, TKE, etc. $M_{\rm CP}$ and $M_{\rm IMF}$ distributions are shown in fig. 2a) and fig. 2b), for all the selected events. As described below, most of the complete events (84% of the total) consist of reactions with two or three fragments in the exit channel, *i.e.* corresponding to binary or ternary reactions in semi-peripheral collisions.

To further characterize these complete events, the correlation between the longitudinal component (*i.e.* along the beam axis) of the velocity, $v_{\rm par}$, and the mass number, A, for

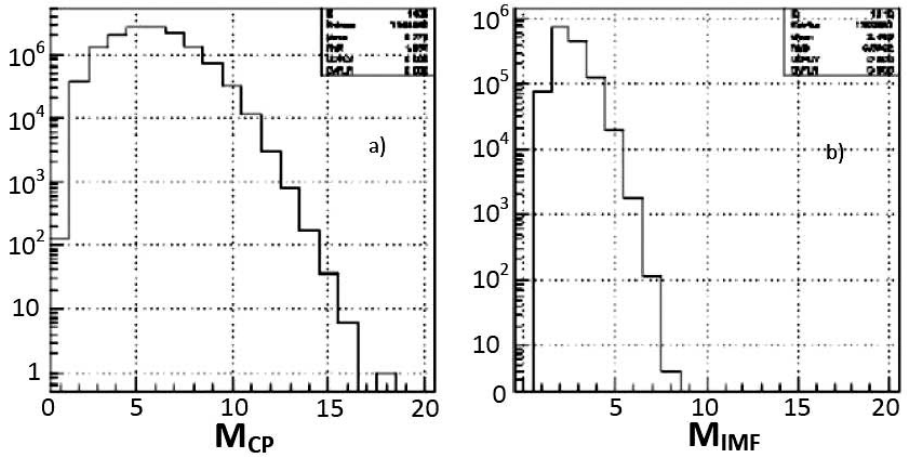

Fig. 2. – Charged particles multiplicity $M_{\rm CP}$ (on the left) and fragments multiplicity $M_{\rm IMF}$ (on the right) distributions for all complete events.

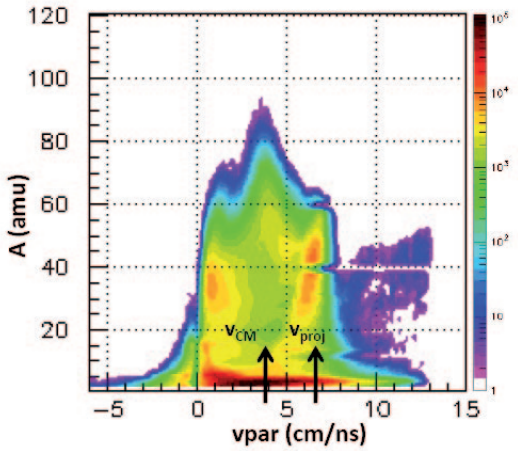

Fig. 3. – Correlation between the longitudinal component (*i.e.* along the beam axis) of velocity, v_{par} (cm/ns) and mass, A (a.m.u.), for all detected reaction products in complete events.

all the detected reaction products is constructed (see fig. 3). A large number of fragments with velocity values close to projectile's velocity ($v_{\mathrm{proj}} \approx 6.5\,\mathrm{cm/ns}$) and masses around 40–45 a.m.u. are observed and can be associated to projectile's remnant fragment (PLF). Similarly, a relevant contribution of slow moving fragments corresponding to target's remnant fragments (TLF), is observed. A broad component of fragments with velocities centered around the centre-of-mass velocity, $v_{\mathrm{CM}} \approx 3.8\,\mathrm{cm/ns}$, and masses larger than projectile or target masses are also evident, indicating the presence of massive residues (produced in complete or incomplete fusion reactions).

3˙2. *Selection of central collisions*. – Since we were interested in studying central collisions, a filter on the energy dissipated in the reaction was applied. A simple selection by means of charged particle multiplicity was in fact not enough to fully characterize the most central collisions. Therefore, we have chosen to adopt a more stringent selection method, based on imposing restrictive cuts on the global variables, event-by-event, Total Kinetic Energy (TKE), measured as the sum of the kinetic energy of each detected fragment, and the flow angle, $\vartheta_{\mathrm{flow}}$. This latter variable was built starting from the Cartesian coordinates of the measured linear momenta, in the center-of-mass frame, of all the IMFs detected in each event. The kinetic flow tensor, Q_{ij}, was built event by event, as follows:

$$Q_{ij} = \sum_{Z \geq 3} \frac{p_i p_j}{2m(Z)}. \tag{1}$$

This tensor is a generalization of the sphericity tensor, widely used in high energy particle physics and adapted to nuclear reactions in which composite fragments are produced. In its diagonal form Q_{ij} defines an ellipsoid in momentum space with the three principal axes oriented along the three eigenvectors, whose corresponding eigenvalues f_1, f_2, and f_3, are sorted and ordered according to the inequalities, $f_1 > f_2 > f_3 > 0$ [6-10], in a way that the orientation of the main axis of the ellipsoid (eigenvector corresponding to f_1) measured with respect to the direction of the incident beam defines the flow angle

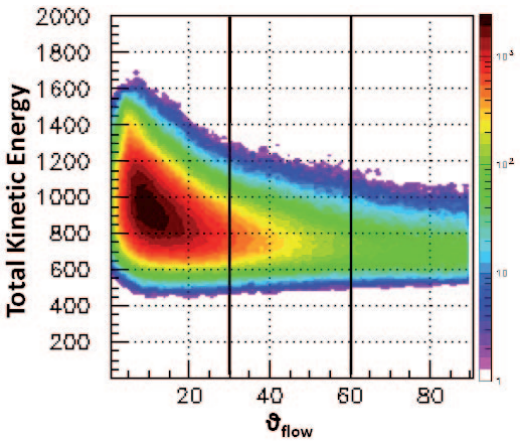

Fig. 4. – Total Kinetic Energy (TKE) and $\vartheta_{\rm flow}$ angle correlation, for all the complete events.

$\vartheta_{\rm flow}$. The angle $\vartheta_{\rm flow}$ characterizes the shape of the event in momentum space. Briefly, for peripheral and semi-peripheral collisions this ellipsoid has the tendency to be aligned along the beam direction, and consequently, $\vartheta_{\rm flow}$ assumes small values approaching 0 degrees. On the contrary, for more dissipative and central collisions a more spherical shape of the ellipsoid is expected; so that, $\vartheta_{\rm flow}$ will assume larger values, up to 90 degrees.

Therefore, a good selection of central collisions, as already performed in ref. [3], could be checked by means of graphic cuts on Total Kinetic Energy (TKE) and $\vartheta_{\rm flow}$ correlation [11], as is shown in fig. 4.

In the following, less dissipative collisions (high values of TKE) are cut off from the analysis when $\vartheta_{\rm flow} > 60°$.

Following the pattern of $v_{\rm par}$-A correlation for all the reaction products with increasing $\vartheta_{\rm flow}$ values, through the three regions $\vartheta_{\rm flow} \leq 30$, $30° < \vartheta_{\rm flow} \leq 60°$, $\vartheta_{\rm flow} > 60°$ in fig. 5, it is evident a steady decrease of PLF and TLF contributions. For values of $\vartheta_{\rm flow} > 60°$, fragments with velocities close to the center-of-mass velocity and masses

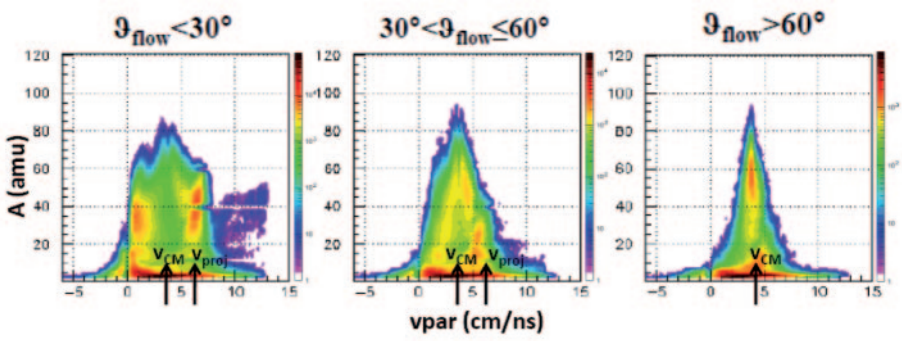

Fig. 5. – Correlation between parallel velocity component (cm/ns) and mass (a.m.u.) for all reaction products in the three regions: $\vartheta_{\rm flow} \leq 30°$ (on the left), $30° < \vartheta_{\rm flow} \leq 60°$ (in the middle), $\vartheta_{\rm flow} > 60°$ (on the right).

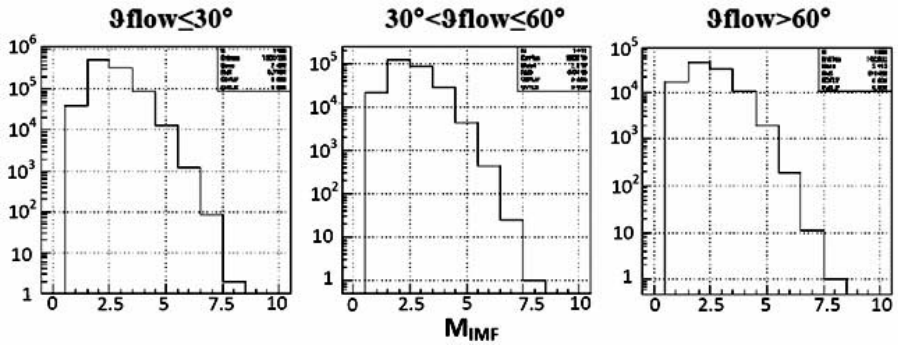

Fig. 6. – IMF multiplicity ($M_{\rm IMF}$) distributions for the three different gates on flow angle values.

exceeding 60 a.m.u. are clearly observed.

The presence of these latter fragments is a strong indication of the formation of massive residues coming from fusion-evaporation processes. Figure 6 shows the evolution of the IMF multiplicity for three different gates on $\vartheta_{\rm flow}$ values. In the case of $\vartheta_{\rm flow} > 60°$, one observes a high yield of events with only one IMF in the exit channel and the persistence of events with high IMF multiplicity ($M_{\rm IMF} \geq 4$).

3˙3. *Single source events selection.* – Since we were interested to investigate the competition between different reaction mechanisms, namely, fusion-evaporation and multifragmentation for the reaction in study, it was necessary to isolate events from a single source created by the complete overlap of projectile and target nuclei in the collision. In fact, it is well established from previous studies that a non-negligible component of the dominant binary reactions, reminiscent of deep inelastic collisions or incomplete fusion reactions, may exist in the above selection, also in the region of high IMF multiplicity events. Indeed, a contribution of events with $M_{\rm IMF} = 2$ and fragment's mass between 20 and 40 a.m.u. is observed in fig. 5 and for $\vartheta_{\rm flow} > 60°$.

In order to better study this latter observation a more restrictive selection was adopted, by means of an additional gate on the global TKE variable on the selected central events. It was observed that the additional condition TKE < 700 MeV strongly reduces the above-mentioned fragments with mass values between 20 and 40 a.m.u. and velocities close to that of the center of mass. Therefore, we focused on the most dissipative central events, selected as those events with TKE < 700 MeV and $\vartheta_{\rm flow} > 60°$ (fig. 7). The $v_{\rm par}$-A correlation plot for events with TKE < 700 MeV is shown in fig. 8. In that case we also observe an increasing relative yield of events where one fragment is detected in coincidence with, on average, four light particles ($Z < 3$) (see fig. 9). A comparison between $M_{\rm IMF}$ distributions, normalized to total number of events, for central ($\vartheta_{\rm flow} > 60°$, black full line) and more dissipative central (TKE < 700 MeV and $\vartheta_{\rm flow} > 60°$, red full line) collisions is shown in fig. 9: a relevant component with high values of $M_{\rm IMF}$ is present in both distributions, providing a first indication of the coexistence of both massive residues from fusion-evaporation reaction and multifragmentation-like phenomena.

In fig. 10, it is also worth showing the $v_{\rm par}$-$v_{\rm per}$ correlation plot (where $v_{\rm per}$ is the component of fragment velocity perpendicular to beam axis in the laboratory reference system, measured by TOF technique), for the most dissipative central collisions described

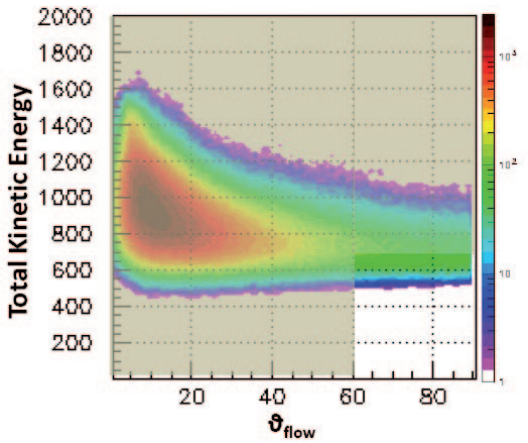

Fig. 7. – More restrictive selection by means of an additional gate on the global TKE variable for selected central events.

above. The location of the events in such a plot is consistent with the emission of fragments from a well-defined unique source with velocity values close to the center-of-mass velocity. A simple evaluation of the mass of this source (just by adding all the detected charge and correcting for the undetected evaporated neutrons) provides a value around 88 a.m.u., very close to the mass corresponding to the complete overlap of projectile and target nuclei.

3˙4. *Evidence for fusion-evaporation and multifragmentation reaction mechanisms.* – In this section a more stringent characterization of the above-described dissipative central collisions (TKE < 700 MeV and $\vartheta_{\rm flow} > 60°$) is performed.

In order to better explain the observations in fig. 8, the $v_{\rm par}$-A correlation for the

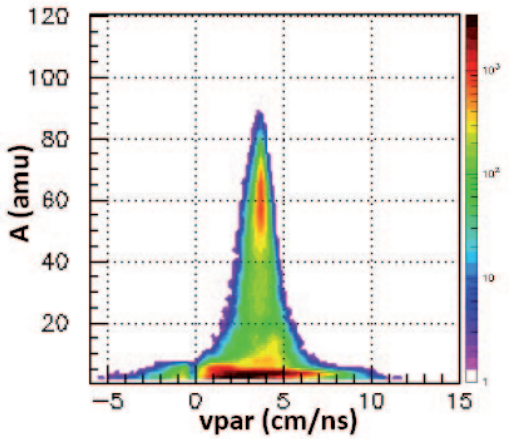

Fig. 8. – $v_{\rm par}$-A correlation for all reaction products in the most dissipative central collisions (TKE < 700 MeV and $\vartheta_{\rm flow} > 60°$).

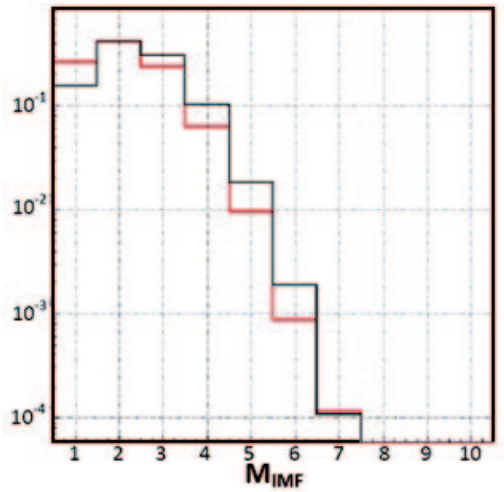

Fig. 9. – (Colour on-line) Comparison between M_{IMF} distributions, normalized to total number of events, for central ($\vartheta_{\mathrm{flow}} > 60°$) and dissipative central (TKE $< 700\,\mathrm{MeV}$ and $\vartheta_{\mathrm{flow}} > 60°$) collisions.

largest fragment in each event represented in fig. 8 is shown in fig. 11. This way we can isolate events with only one heavy residue in the exit channel. These latter events represent about 60% (fig. 11a) of the whole selected data.

More quantitatively, the biggest fragment with mass 50 a.m.u. or larger is preferentially emitted as a unique heavy IMF (43.5% of events on the upper panel of fig. 11) in coincidence with 4-5 light charged particles ($Z = 1$, $Z = 2$) or, alternatively, together with a few (1-2) light IMF. This behavior, that is strongly indicative of a complete fusion process, can be further investigated by inspecting the diagram of fig. 12a, where the mass distributions of the three biggest fragments for such "fusion-evaporation" events (fig. 11a) are reported.

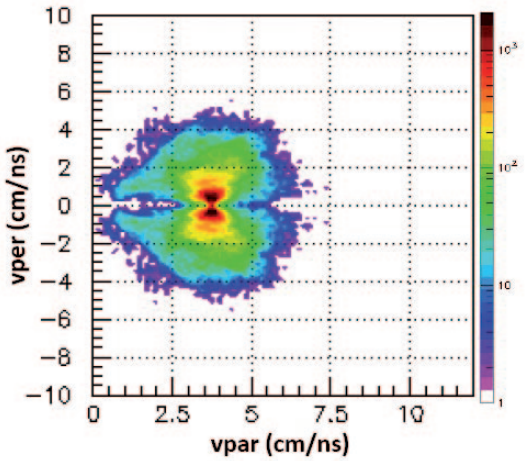

Fig. 10. – v_{par}-v_{per} correlation plot for all fragments detected in the most dissipative central events.

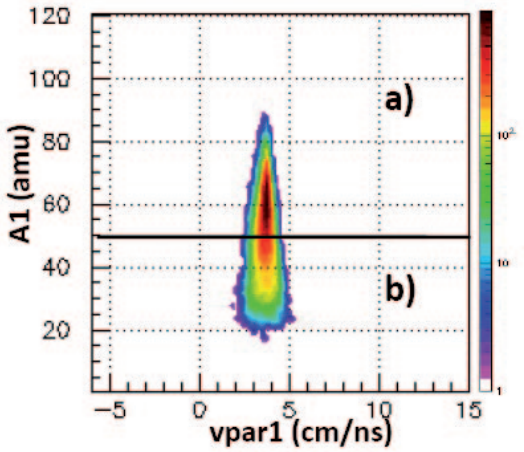

Fig. 11. – $v_{\rm par}$-A correlation for the largest fragment present in each event represented in fig. 10.

In contrast, by inspecting the data in fig. 11b, corresponding to most dissipative central events that do not show any presence of a heavy residue, it is possible to realize that the fragment multiplicity $M_{\rm IMF}$ spans a substantially wider range of values, with a mean of $\langle M_{\rm IMF}\rangle = 3$, and reaching maximum values as high as $M_{\rm IMF} = 6$. For these events, the light charged particle multiplicity is lowered to a mean value of about three particles per event.

The method described above, allows for a stringent signature of a multifragmentation process. This signature is strongly supported by the plots shown in fig. 12a and fig. 12b, where three differently colored curves, representing the mass distributions of three biggest

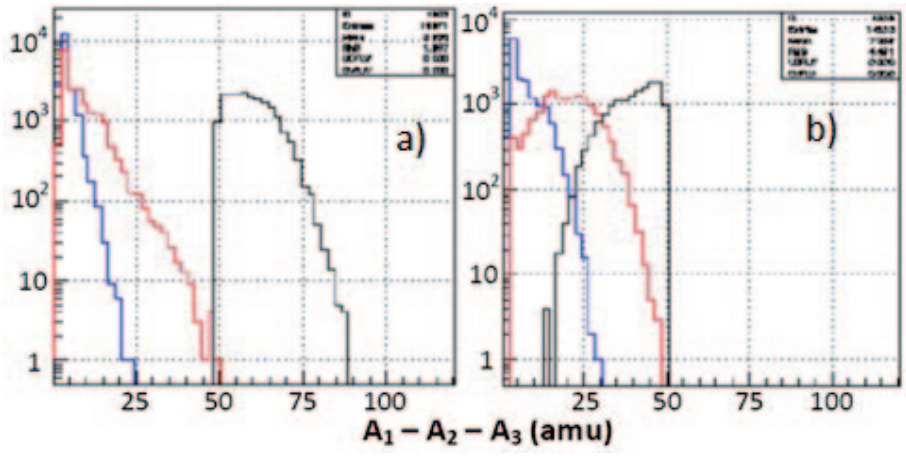

Fig. 12. – (Colour on-line) a) Mass distributions of the three heavier fragments for events with a fusion-evaporation like residue (events in fig. 11a); b) the same distributions for multifragmentation-like events (in fig. 11b). Different colors correspond to different types of fragments: the heaviest, the second, and the third massive fragments.

fragments emitted in each event, display the characteristic features of typical fusion phenomena (fig. 12a) and of typical multifragmentation events (fig. 12b) characterized by a clear tendency towards the splitting of the composite system in fragments with equal masses [12].

However, it is important to notice that the division that was performed in fig. 11, corresponding to mass values of 50 u.m.a., in order to separate events characterized by an evaporation like process from multifragmentation ones, is, at the moment, only an arbitrary cut characteristic of preliminary analyses. Therefore, a more careful analysis is in progress in order to evaluate the cross-sections associated to each of the two main reaction mechanisms.

4. – Conclusion

The main features of the reaction products in $^{58}\mathrm{Ni} + ^{48}\mathrm{Ca}$ central collisions at $E_{\mathrm{lab}}(\mathrm{Ni}) = 25\,A\mathrm{MeV}$, performed at LNS by using the 4π CHIMERA multidetector, have been studied in order to investigate the competition between different reaction mechanisms. By means of the construction of the kinetic energy tensor and the flow angle in each complete event, central collisions have been selected. A large contribution of events with a heavy residue in coincidence with a high multiplicity of light charged particles (5 on average) has been observed. This study has shown also the presence of another class of central events with a larger IMF multiplicity and a smaller number of light charged particles (about 3). Further analyses will be performed in order to obtain a quantitative evaluation of the cross-sections associated to different processes.

* * *

The author wishes to thank CHIMERA Collaboration for the help given during data analysis. The author is also grateful to G. Verde and B. Tsang for their carefully reading of the manuscript.

REFERENCES

[1] Lynch W. G., *Nucl. Phys. A*, **583** (1995) 471.
[2] de Souza R. T., Le Neindre N., Pagano A. and Schmidt K.-H., *Eur. Phys. J. A*, **30** (2006) 275.
[3] Geraci E. *et al.*, *Proceedings of the IWM2009, International Workshop on Multifragmentation and related topics, Catania – Italy, November 2009* (pp. 30-36).
[4] Pagano A. *et al.*, *Nucl. Phys. A*, **734** (2004) 504.
[5] Pagano A. (for the CHIMERA Collaboration), *Proposal for upgrading CHIMERA 4π detector*, *Proceedings of the XLII International Winter Meeting on Nuclear Physics, Bormio – Italy, March 2005*, pp. 150-155.
[6] Gyulassy M. *et al.*, *Phys. Lett. B*, **110** no. 3, 4 (1982).
[7] Herrman *et al.*, *Annu. Rev. Nucl. Part. Sci.*, **49** (1999) 581.
[8] Cugnon J. *et al.*, *Nucl. Phys. A*, **397** (1983) 519.
[9] Stocker H. *et al.*, *Nucl. Phys. A*, **387** (1982) 205c.
[10] Stocker H. and Greiner W., *Phys. Rep.*, **137** (1986) 277.
[11] Lecolley J. F. *et al.*, *Phys. Lett B*, **387** (1996) 460.
[12] L. Francalanza, Tesi di Laurea Specialistica in Fisica Nucleare e Subnucleare, A.A. 2010-2011.